Biochimica et Biophysica Acta 861 (1986) 267–276
Elsevier

BBA 73304

Subcellular distribution of ATP-dependent calcium transport in rat duodenal epithelium

Emile J.J.M. van Corven [a,*], Carel H. van Os [b] and Austin K. Mircheff [a]

[a] *Department of Physiology and Biophysics, University of Southern California, School of Medicine, Los Angeles, CA 90033 (U.S.A.) and* [b] *Department of Physiology, University of Nijmegen, P.O. Box 9101, 6500 HB Nijmegen (The Netherlands)*

(Received 4 April 1986)

Key words: Ca^{2+}-ATPase; Ca^{2+} transport; Counter-current distribution; Subcellular localization; (Rat small intestine)

Subcellular fractionation studies were performed to delineate plasma membrane and intracellular membrane populations which might be involved in intracellular Ca^{2+}-homeostasis of rat small intestinal epithelial cells. After a low-speed supernatant fraction had been suspended in 5% sorbitol and subjected to equilibrium centrifugation in a zonal rotor, the Golgi and endoplasmic reticulum markers, galactosyltransferase and NADPH–cytochrome *-c* reductase, were concentrated in a density region designated Window II. The basal-lateral membrane marker (Na^+-K^+)-ATPase was concentrated in a higher-density region designated Window III. ATP-dependent Ca^{2+} transport was equally distributed between the two windows. Several membrane populations could be resolved from each window with good recovery of Ca^{2+}-transport activity by a second density gradient centrifugation step. Second density gradient fractions were subjected to counter-current partitioning in an aqueous polymer two-phase system. Basal-lateral membranes, characterized by an 11-fold enrichment of (Na^+-K^+)-ATPase, contained ATP-dependent Ca^{2+}-transport activity with $V_{max} = 3.7$ nmol/mg per min and $K_m = 0.5$ μM. A major Golgi-derived population exhibited Ca^{2+}-transport activity with V_{max} and K_m values similar to those of the basal-lateral membranes. One membrane population, presumed to have been derived from the endoplasmic reticulum, contained Ca^{2+}-transport activity with $V_{max} = 4$ nmol/mg per min and $K_m = 0.5$ μM. In addition to demonstrating that ATP-dependent Ca^{2+}-transport activity has a complex distribution within enterocytes, this study raises the possibility that the basolateral plasma membranes might account for a relatively minor portion of the cell's Ca^{2+}-pumping ability.

Introduction

The ability of the small intestinal epithelium to actively absorb calcium ions has been appreciated for many years. Several laboratories [1–3] have demonstrated Ca^{2+}-ATPase and ATP-dependent Ca^{2+}-transport activities in isolated basolateral membrane samples. These results have been incorporated into a model for active absorption of Ca^{2+} involving passive, facilitated entry across the apical plasma membranes, diffusion through the

* Permanent address: Department of Physiology, University of Nijmegen, P.O. Box 9101, 6500 HB Nijmegen, The Netherlands.

Abbreviations: EGTA, ethylene glycol bis(β-aminoethyl ether)-*N*,*N*′-tetraacetic acid; HEEDTA, *N*-(2-hydroxyethyl)ethylenediamine-*N*,*N*′,*N*′-triacetic acid; Hepes, 4-(2-hydroxyethyl)-1-piperazineethanesulphonic acid; PMSF, phenylmethanesulphonyl fluoride.

Correspondence address: Dr. C.H. van Os, Department of Physiology, University of Nijmegen, P.O. Box 9101, 6500 HB Nijmegen, The Netherlands.

cytoplasm, and ATP-driven efflux across the basolateral plasma membranes.

More recently, it has become clear that intestinal epithelial cells, like the cells of other tissues, employ Ca^{2+} as an intracellular messenger. Donowitz et al. [4] have shown that dantrolene, which blocks the release of Ca^{2+} from intracellular pools, increases Na^+ and Cl^- absorption by rabbit ileum. This result indicates that in intestinal epithelial cells, as in exocrine acinar cells, uptake and release of Ca^{2+} by one or more intracellular pools play key roles in cellular Ca^{2+} metabolism. However, very little is known about the enterocyte's intracellular calcium storage sites.

We have employed techniques of analytical fractionation to survey the subcellular distribution of ATP-dependent Ca^{2+}-transport activity in duodenal villus cells. We find that this activity is present in a wide variety of membrane populations. In addition to the basolateral membranes, it can be detected in populations which can be identified as having been derived from the endoplasmic reticulum and from the Golgi complex.

Materials and Methods

Isolation and homogenization of enterocytes

Four overnight-fasted male Sprague-Dawley rats (180–200 g) were killed by cervical dislocation. The duodena (15-cm pieces) were removed and rinsed with ice-cold 150 mM NaCl, pH 7.4, with 1 mM dithiothreitol. Everted pieces were tied onto rods and vibrated at 4°C in 150 mM NaCl, 1 mM dithiothreitol with low amplitude (2 mm) and high frequency (60 Hz). After the first minute, shed debris was discarded. The villus cells were collected after an additional hour of vibration in 150 mM NaCl, 2.5 mM EDTA, pH 7.4, with 1 mM dithiothreitol. Cells were pelleted at $200 \times g$ for 10 min, resuspended in 5% sorbitol, 0.5 mM Na_2-EDTA, 5 mM histidine/imidazole, pH 7.5 (plus 1 mM dithiothreitol, 0.2 mM PMSF and 8.6 μg/ml aprotinin). The cells were homogenized for 10 min at a low speed setting of a Tissumiser (Tekmar Instruments) as described previously [5]. After centrifugation ($1000 \times g$ for 10 min) the pellet was homogenized and centrifuged again. The final low-speed pellet was designated P_0, and the pooled supernatant S_0. S_0 was immediately subjected to equilibrium density centrifugation in a zonal rotor.

Equilibrium density centrifugation

The zonal rotor (Beckman Z-60) was loaded in the following sequence: an overlay of 10 ml 5% sorbitol buffer, 50 ml of S_0 in 5% sorbitol, a hyperbolic gradient formed by delivering 250 ml 65% sorbitol through a constant-volume mixing chamber initially loaded with 180 ml of 30% sorbitol and a cushion of 25 ml 80% sorbitol. After centrifugation at $240\,000 \times g$ for 70 min, the rotor contents were displaced with 80% sucrose and collected in 24 fractions. The density gradient fractions were diluted to 26 ml with 5% sorbitol and centrifuged at $250\,000 \times g$ for 60 min. The resulting pellets collectively designated (ΣP_i) were resuspended in 3 ml of 5% sorbitol buffer. All sorbitol buffers contained 0.5 mM Na_2-EDTA, 5 mM histidine/imidazole, pH 7.5, except the resuspension buffer. Added fresh were 0.2 mM PMSF and 8.6 μg/ml aprotinin.

Second density gradient centrifugation

Pooled fractions from the first density gradient centrifugation step were brought to 55% sorbitol with an 87.4% sorbitol solution. A 40 ml centrifugation tube was loaded in the following sequence: a hyperbolic gradient formed by delivering 23 ml of 55% sorbitol through a constant-volume mixing chamber initially loaded with 16 ml of 30% sorbitol; 9.42 g of sample (in 55% sorbitol); 3 ml of 55% sorbitol and a cushion of 3 ml 65% sorbitol. For equilibrating the tubes, 5% sorbitol was added on top of the gradient. After centrifugation ($55\,000 \times g$ for 240 min) in a Beckman SW28 rotor, six fractions were collected, diluted with 5% sorbitol without EDTA, pelleted ($250\,000 \times g$ for 60 min) and resuspended in 3 ml of 5% sorbitol without EDTA.

Counter-current distribution

Counter-current distribution was performed at 4°C in a thin-layer apparatus as described previously [5–8]. The phase system contained 5% Dextran T-500, 3.6% poly(ethylene glycol)6000, 10 μM EDTA and 8.33 mM imidazole, pH 6.5 adjusted with HCl. The systems were allowed to

equilibrate overnight at 4°C before separation of upper and lower phases.

Analytical methods

Marker enzyme and protein determinations were performed with the same methods used in previous studies [9]. Ouabain-sensitive K^+-stimulated *p*-nitrophenylphosphatase is measured instead of (Na^+-K^+)-ATPase. Marker incremental enrichment factors resulting from individual separation procedures were calculated as the ratios of percentage of recovered marker to percentage of recovered protein. Marker cumulative enrichments were calculated as the products of the incremental enrichment factors obtained in each of the sequence of separation steps [9].

Ca^{2+}-uptake was measured at 37°C with a rapid filtration technique as described before [10]. The mitochondrial inhibitors oligomycin (5 μg/ml) and NaN_3 (1 mM) were routinely added to the Ca^{2+}-uptake media which contained 1 μM Ca (free), 5 mM $MgCl_2$, 150 mM KCl, the Ca^{2+} buffers EGTA (0.5 mM) and HEEDTA (0.5 mM). The pH was maintained at 7.4 with 20 mM Hepes/Tris.

Materials

Tris-ATP, oligomycin, EGTA, HEEDTA, PMSF, aprotinin and dithiothreitol were from Sigma (St. Louis). Dextran T500 was from Pharmacia (Uppsala, Sweden) and poly(ethylene glycol)6000 was from Union Carbide (New York). $^{45}CaCl_2$ (10 mCi/mg) was from New England Nuclear. All other chemicals were at least analytical grade and were obtained from standard suppliers.

Results

The distributions of enzymatic markers among the differential sedimentation fractions are given in Table I. Apart from maltase, the relevant enzymatic markers are present in the highest amounts in ΣP_i. The relatively larger amounts of maltase in the low-speed pellet, P_0, probably represent intact brush border fragments [5].

Fig. 1 summarized the four marker enzymes of interest and ATP-dependent Ca^{2+}-uptake distributions observed after S_0 was subjected to equilibrium centrifugation in the Z-60 zonal rotor. As found in analytical fractionation of jejunal epithelial cells, all of the markers but succinate dehydrogenase, a mitochondrial inner membrane marker, have complex distributions which indicate that each is associated with two or more distinct membrane populations [5]. The peak of maltase (not shown) centered in fraction 22 represents brush border membranes [5]. This population overlaps the mitochondria (not shown) and a high-density, complex aggregate, which is indicated by the coinciding peaks of all markers in fraction 23. On the basis of the distribution of (Na^+-K^+)-ATPase, a conventional basolateral membrane marker, and galactosyltransferase, a conventional Golgi marker, we designated gradient fractions 6–11 as Density Window II and fractions 13–17 as Density Window III. Window II contained 25% of the initial galactosyltransferase activity, while Density Window III contained 30% of the initial (Na^+-K^+)-ATPase activity.

ATP-dependent Ca^{2+}-transport activity, like NADPH–cytochrome-*c* reductase, was distributed approximately evenly between the two density windows. This activity cannot be the result of mitochondrial contamination, since mitochondria

TABLE I

DISTRIBUTION OF ENZYMATIC MARKERS AMONG THE DIFFERENTIAL SEDIMENTATION FRACTIONS

Mean values ± S.D. are given of percentage yields of total activities recovered among the differential sedimentation fractions. Yield in P_0 was calculated from $(P_0 \times 100)/(P_0 + S_0)$. Values of ΣS_i and ΣP_i are expressed in terms of 100% recovery from S_0. Yield in ΣP_i was calculated from ($\Sigma P_i \times$ percentage in S_0)/($\Sigma P_i + S_i$). Actual recoveries of S_0 after zonal centrifugation are also given (last row). Protein and (Na^+-K^+)-ATPase values are the means of six experiments, galactosyltransferase of three experiments and the rest of four experiments.

	P_0	ΣS_i	ΣP_i	Recovery
Protein	28.5 ± 6.9	46.4 ± 14.4	26.3 ± 12.1	81.2
(Na^+-K^+)-ATPase	30.4 ± 6.9	6.4 ± 5.0	63.2 ± 15.0	61.5
Maltase	53.8 ± 13.6	34.2 ± 9.9	12.0 ± 7.8	161.7
NADPH cyt-*c*-red.	30.3 ± 13.0	20.4 ± 27.3	49.3 ± 10.0	40.6
Galactosyltransf.	29.0 ± 19.0	38.4 ± 29.5	44.0 ± 16.9	76.1

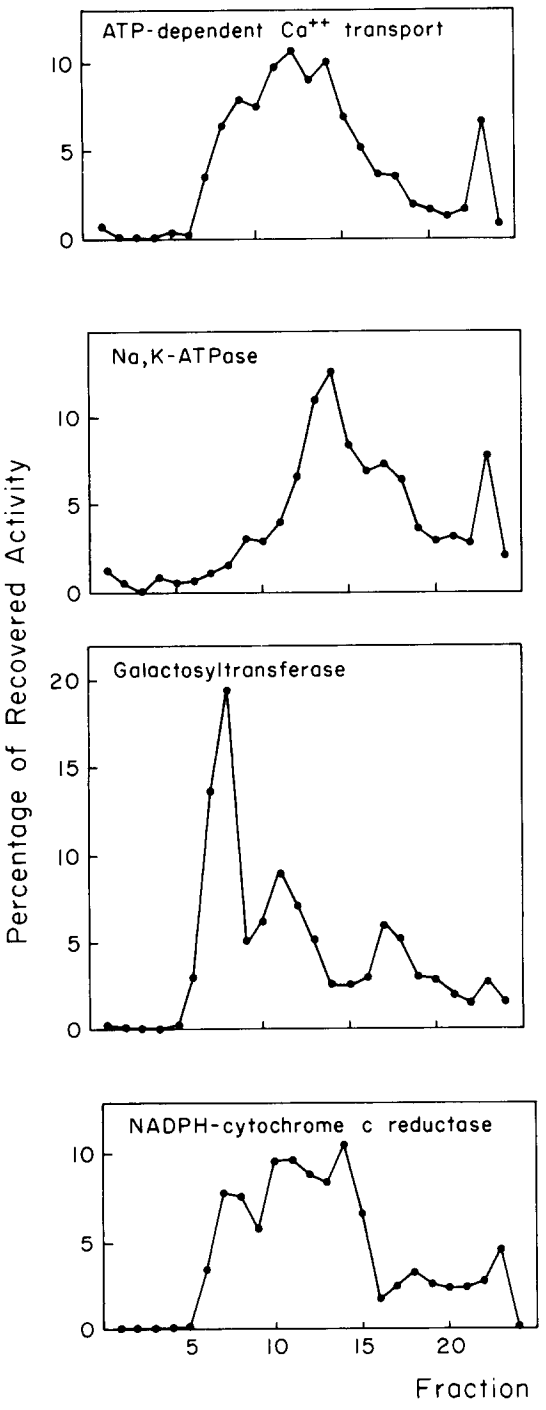

Fig. 1. Density distributions of ATP-dependent Ca^{2+} uptake, protein and enzymatic markers. Density gradient centrifugation was performed in a Z-60 zonal rotor as described under Methods.

were essentially absent from this region of the density gradient, and since the transport measurements were made in media containing the mitochondrial inhibitors NaN_3 and oligomycin. The distribution of transport activity in Fig. 1 substantiates the observation of Rubinoff and Nellans [11] that ATP-dependent Ca^{2+}-transport activity was associated with other membranes in addition to the basolateral membranes. Since Window II contained peaks of both galactosyltransferase and NADPH–cytochrome-*c* reductase, it seemed likely that it contained both Golgi and endoplasmic reticulum populations. However, it was not possible to delineate all the component populations in Window II solely on the basis of marker distributions such as those presented in Fig. 1. A similar problem was presented by the marker distribution patterns in Density Window III. This window contained peaks of galactosyltransferase and NADPH–cytochrome-*c* reductase in addition to $(Na^+\text{-}K^+)$-ATPase, so it seemed likely that a mixture of Golgi, endoplasmic reticulum, and basolateral membranes was present in Window III. However, it was not possible to delineate these populations or to determine how the ATP-dependent Ca^{2+}-transport activity might be distributed among them.

In Fig. 2 a time course of Ca^{2+}-uptake by membranes from density Window II is shown. Addition of the Ca^{2+}-ionophore A23187 resulted within 15 s in release of 90% of accumulated Ca^{2+}, indicating uptake against a concentration gradient. The same time course and A23187 effect were

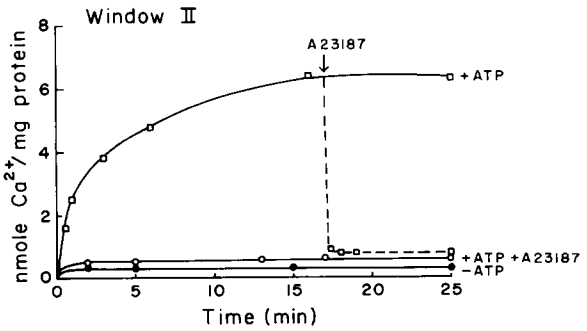

Fig. 2. Time course of Ca^{2+} uptake in the presence and absence of 10 mM ATP. Pooled membrane fraction from Density Window II (fractions 6–11) and III (fractions of 13–17) were used. (Results of Window III not shown.)

observed for membranes from Density Window III.

Counter-current distribution analyses of membranes from Window II and Window III (data not shown) confirmed that each Window contained a multiplicity of membrane populations. It would be necessary to postulate at least four separate populations to account for the observed marker distributions in Window II. Similarly, the marker distributions after counter-current distribution of Window III would suggest the presence of at least three membrane populations. ATP-dependent Ca^{2+}-transport activity appeared to be associated with each of the populations from both density windows. Thus, only about half the ATP-dependent Ca^{2+}-transport activity recovered after counter-current distribution of Density Window III was associated with the peak of $(Na^{+}\text{-}K^{+})$-ATPase-rich membranes that would be identified as basolateral membranes.

While the counter-current distribution analyses of Windows II and III confirmed that ATP-dependent Ca^{2+}-transport activity had a complex subcellular distribution, the recovery of transport activity was so low (5 and 7%, respectively) that we could not accurately characterize the activities associated with the various populations. To obtain such information, we devised a second density gradient centrifugation procedure as an alternative, more rapid means of subfractionating Density Windows II and III.

Figure 3 summarizes the marker distribution patterns which resulted when Density Window II was subjected to density gradient centrifugation after its sorbitol concentration had been brought to 55% as described under Methods. The recovery of ATP-dependent Ca^{2+} transport was now 26%, much better than after counter-current distribution. Table II summarizes the corresponding marker enrichment factors. To determine whether fractions obtained in this way might represent reasonably pure samples of particular subcellular membrane populations, we subjected them to counter-current distribution analysis. The analysis of fractions 3, 4 and 5 from the second density gradient centrifugation of Window II are presented as two-dimensional separation in Fig. 4. Window II was more complex than had been anticipated on the basis of the counter-current

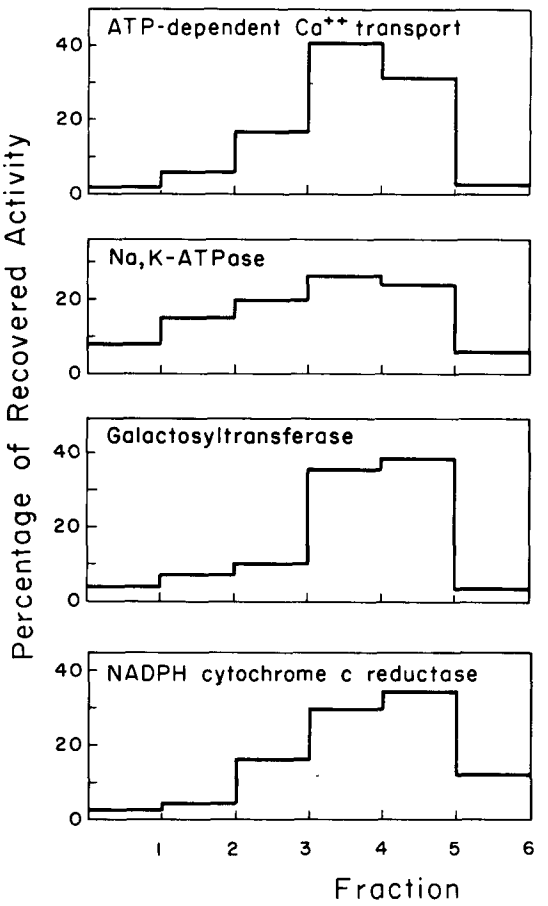

Fig. 3. Density distribution of ATP-dependent Ca^{2+} uptake, protein and enzymatic markers after a second density gradient centrifugation of Density Window II (fractions 6–11 in Fig. 1).

distribution analysis. As summarized in the lower-right panel of Fig. 4, fractions 3, 4 and 5 from the second density gradient subfractionation of Window II contained a total of 10 distinct membrane populations. However, fraction 3 was dominated by a single major population, designated population *h*. Population *h* appeared to be primarily endoplasmic reticulum in character, since it has a relatively greater cumulative enrichment factor for NADPH–cytochrome-*c* reductase than for the other markers tested. Fraction 5 was also dominated by one major population, designated population *e*. Population *e* appeared to be primarily Golgi in character, since it had a relatively greater cumulative enrichment factor for galactosyltransferase; its galactosyltransferase enrichment

TABLE II

NET CUMULATIVE ENRICHMENT FACTORS OF ENZYMATIC MARKERS AFTER SECOND DENSITY GRADIENTS CENTRIFUGATION OF WINDOWS II AND III AND AFTER COUNTER-CURRENT DISTRIBUTION OF SECOND GRADIENT FRACTION

Cumulative enrichment factors relate observed marker specific activities to specific activities in the initial homogenate. The calculations, which include corrections for recovery, were performed as outlined under Methods and described in detail by Mircheff and Lu [16]. Coordinates in parenthesis give locations (Density Window from first gradient, fraction from second gradient, counter-current distribution fractions) of samples used in these calculations.

	(Na^+-K^+)-ATPase	Maltase	NADPH cyt-*c*	Gal. trans
Fraction				
II,3	2.4	0.1	3.4	3.2
II,5	0.8	0.2	2.0	3.2
III,3	8.8	0.2	2.7	1.9
III,6	2.1	0.5	1.9	1.4
Population				
e (II,5,51–60)	1.1	n.d.	1.6	4.0
h (II,3,11–20)	2.3	n.d.	3.5	2.6
l' (III,3,41–50)	10.5	n.d.	2.2	1.8

factor of 4.0 was similar to the factor of 6.1 reported by Walters et al. [12], and its (Na^+-K^+)-ATPase enrichment factor was nearly 5-fold lower. Fraction 4 was more heterogeneous than fractions 3 and 5. It contained two populations, designated *i* and *f*, which resembled each other biochemically but which had slightly different partitioning characteristics; population *b*, which was characterized by a large cumulative enrichment factor for galactosyltransferase; and elements of population *e* spilling over from fraction 5.

Density Window III was subjected to the same two-dimensional analysis as described for Window II. The marker distribution patterns after the second density gradient subfractionation are summarized in Fig. 5, and marker distributions resulting from counter-current distribution analyses of fractions 3, 4 and 5 are presented in Fig. 6. The marker cumulative enrichment factors obtained in these analyses are presented in Table II. The populations designated *l'* and *l''* appeared to represent two slightly different subpopulations of basolateral plasma membranes, since they con-

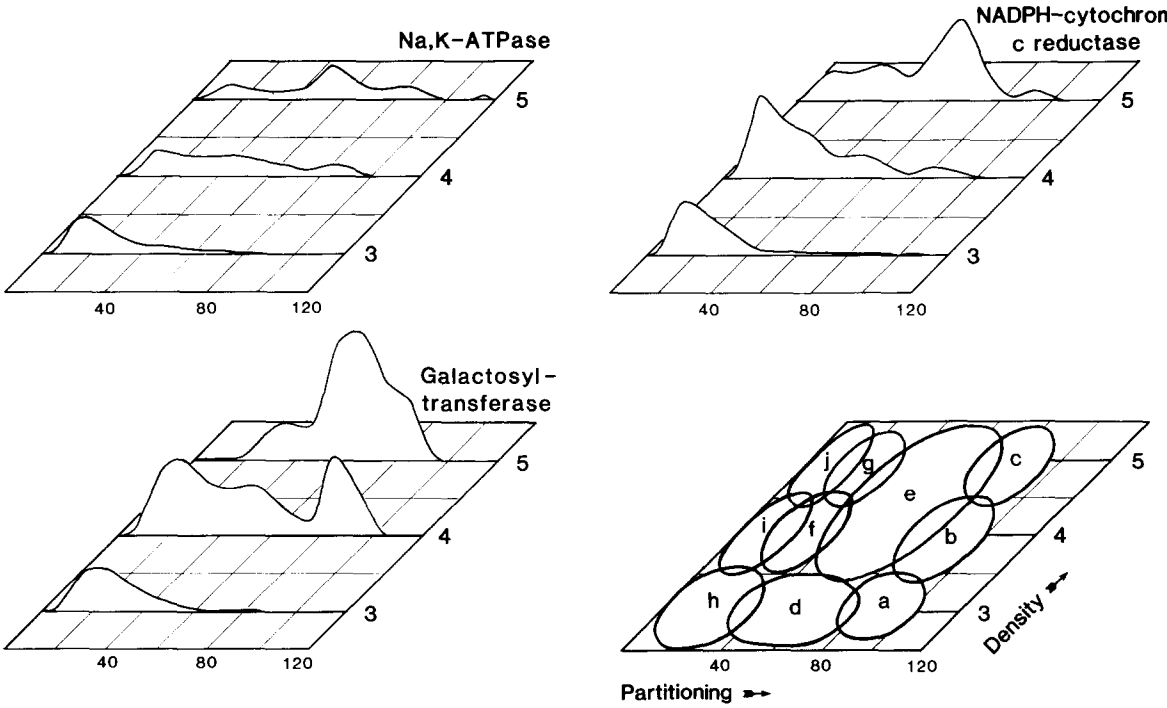

Fig. 4. Summary of second density gradient centrifugation of Window II (*z*-axis) and counter-current distribution analysis of second density centrifugation (*x*-axis) as a two-dimensional fractionation. Elevations above the density partitioning plane (*y*-axis) are proportional to percentages of total recovered activity divided by the number of fractions in the second density gradient.

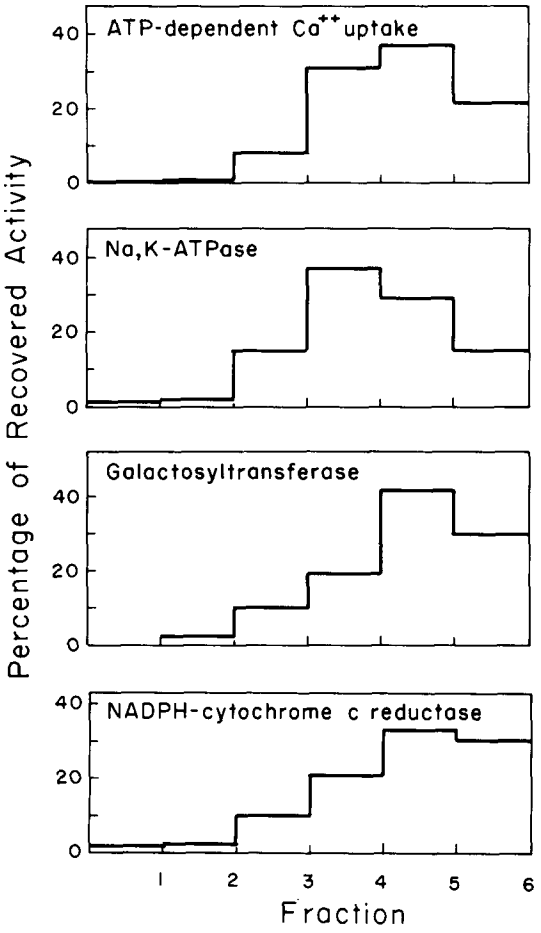

Fig. 5. Density distribution of ATP-dependent Ca^{2+} uptake, protein and enzymatic markers after a second density gradient centrifugation of Density Window III (fractions 13–17 in Fig. 1).

tained the most highly purified (Na^+-K^+)-ATPase activity. Fraction 3 from the second density gradient centrifugation of Density Window III contained a relatively pure sample of population *l'*, while fraction 4 contained an admixture of populations *n* and *l''*. Fraction 5, which was the major locus of ATP-dependent Ca^{2+}-transport activity after the second density gradient centrifugation of Density Window III, was dominated by a major membrane population, designated *m*. The origins of population *m* are not clear, since it exhibited approximately equal net enrichment factors for galactosyltransferase and NADPH–cytochrome-*c* reductase. ATP-dependent Ca^{2+}-transport activity was characterized in fraction 3 from the second density gradient subfractionation of Window III (III, 3), since this fraction represented a relatively pure sample of basolateral membranes, i.e., population *l'*. Fraction III,6 was selected for further analysis because it appeared to represent the subfraction of Density Window III least subject to contamination by the basolateral membrane. Fractions II,3 and II,5 were also selected for further analysis, because they represented relatively pure samples of populations *h* and *e*.

Since the rates of active Ca^{2+} transport were constant for at least 30 s, 30 s uptake values at several Ca^{2+} concentrations were used to estimate the kinetic parameters. Values of K_m and V_{max} obtained by Eadie-Hofstee transformation of the initial rate vs. concentration data are presented in Table III. The apparent K_m values for all four samples were similar (Student's *t*-test, $P > 0.05$). The endoplasmic reticulum sample tested, population *h*, had the highest apparent V_{max}. The Golgi sample tested, population *e*, and the basolateral membrane sample, population *l'*, had intermediate values of V_{max}, and fraction III,6 had the lowest value. The transport activities of the four samples analyzed could not be differentiated on the basis of their apparent K_m values, and differences in V_{max} probably reflect differences in the concentrations of pump sites rather than variability in the intrinsic properties of the pumps. In other preparations it has been possible to distinguish plasma membrane- and endoplasmic reticulum-associated Ca^{2+}-pump activities on the basis of their sensitivities to oxalate [13,14] vanadate and calmodulin [13]. The effects of these agents are summarized in Table IV.

Addition of 1 μM calmodulin to the reaction media had no effect on ATP-dependent Ca^{2+} transport, probably due to the presence of tightly bound endogenous calmodulin [10]. Preincubation of the membrane fractions with the calmodulin antagonist calmidazolium (0.1 μM) dramatically decreased the ATP-dependent Ca^{2+} transport in all four samples. Therefore, the Ca^{2+}-transport activities of both the plasma membranes and the various intracellular membranes appear to have similar interactions with calmodulin. The ATP-dependent Ca^{2+}-transport activities of all four fractions were also similarly stimulated by oxalate.

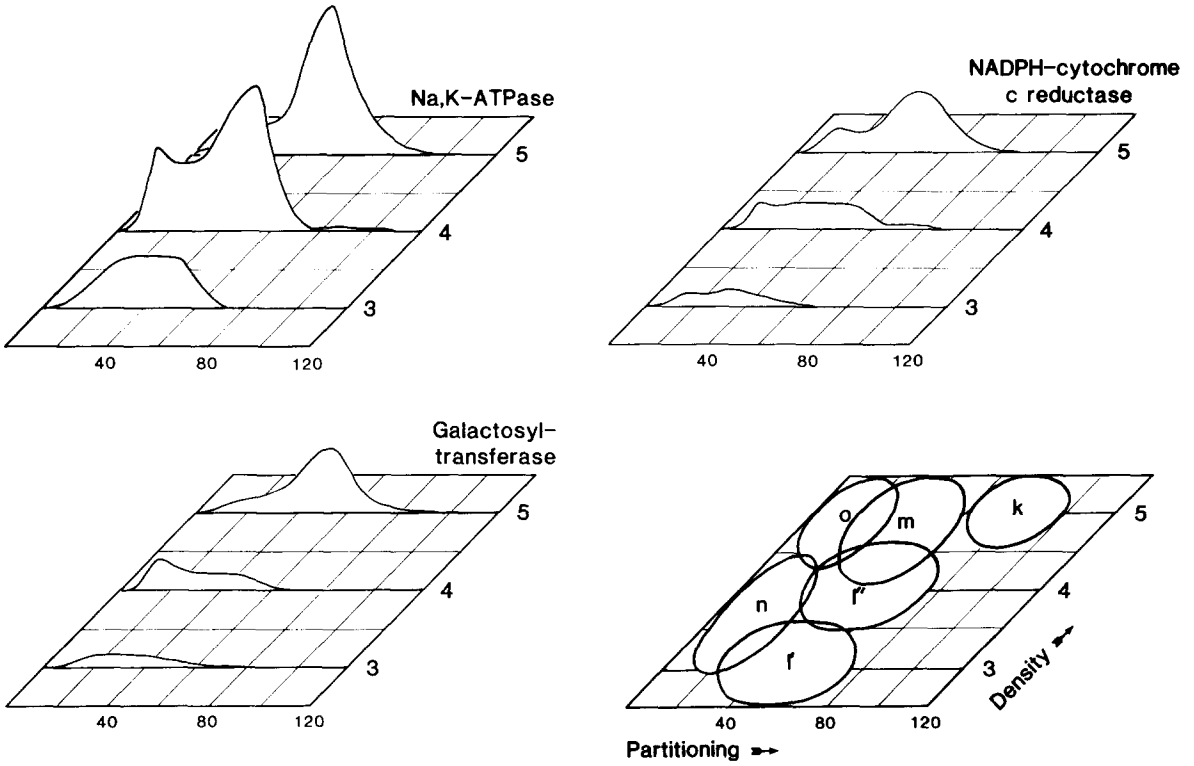

Fig. 6. Summary of second density gradient centrifugation of window III (z-axis) and counter-current distribution analysis of second density gradient fractions (x-axis) as a two-dimensional fractionation. Elevations above the density partitioning plane (y-axis) are proportional to percentages of total recovered activity divided by the number of fractions in the second density gradient.

Sufficiently high concentrations of vanadate (250 μM) could completely inhibit the ATP-dependent Ca^{2+}-transport activity of each of the four frac-

TABLE III

THE KINETIC PARAMETERS K_m AND V_{max} OF ATP-DEPENDENT Ca^{2+} UPTAKE (INITIAL RATES, 0.5 min) OF THE SECOND EQUILIBRIUM DENSITY GRADIENT FRACTIONS II,3, II, 5, III,3 AND III,6

Means ± S.D. are given from three experiments in duplicate.

Fraction	Population	K_m (μM)	V_{max} (nmol Ca^{2+}/mg protein per min)	cc [a]
II,3	*h* (ER)	0.52 ± 0.16	4.79 ± 1.40	0.93 ± 0.03
II,5	*e* (G)	0.32 ± 0.02	2.24 ± 0.36	0.98 ± 0.02
III,3	*l'* (BLM)	0.52 ± 0.17	3.72 ± 1.23	0.91 ± 0.07
III,6		0.28 ± 0.06	1.63 ± 0.35	0.87 ± 0.06

[a] Correlation coefficient of Eadie-Hofstee analysed data.

TABLE IV

INFLUENCE OF OXALATE, VANADATE, CALMODULIN AND CALMIDAZOLIUM ON ATP-DEPENDENT Ca^{2+} UPTAKE OF THE SECOND GRADIENT FRACTIONS II,3, II,5, III,3 AND III,6

Membranes were preincubated for 1 h on ice with vanadate, calmodulin and calmidazolium. ATP-dependent Ca^{2+} uptakes were done for 0.5 min, except for oxalate, which was tested under steady-state conditions (12 min). Mean percentage inhibition or stimulation is expressed from two experiments in duplicate.

Fraction	Population	Oxalate (10 mM)	Vanadate (1 μM)	Calmodulin (1 μM)	Calmidazolium (0.1 μM)
II,3	*h* (ER)	66.1	−38.0	9.2	−72.4
II,5	*e* (G)	88.5	−27.3	0.1	−87.7
III,3	*l'* (BLM)	68.7	−7.8	−7.1	−75.2
III,6		79.2	−52.8	10.2	−86.7

tions (data not shown). However, fraction III,3, the basolateral membrane sample, had a lower affinity for vanadate, since it was reduced by only 7.8% at 1 μM vanadate, a concentration which inhibited 27.3–52.8% of the activities of the intracellular samples.

Discussion

The results of this study indicate that ATP-dependent Ca^{2+}-transport activity has a complex subcellular distribution, being present in basolateral membranes, several subpopulations of endoplasmic reticulum membranes, and several subpopulations of Golgi membranes. This conclusion was anticipated by previous studies of intestinal epithelial cells [11,12], and the complexity of the Ca^{2+}-transport distribution is reminiscent of the subcellular distributions of enzymatic markers found in surveys of a variety of epithelial cells [5,16–18].

The previous reports that epithelial cell plasma membrane enzymes and transport functions are present in endoplasmic reticulum and Golgi membranes have been interpreted in terms of the concepts of membrane biogenesis and recycling. Thus, aminooligopeptidases detected in endoplasmic reticulum and Golgi membranes were shown to represent different stages in the biosynthesis and assembly of the brush border enzyme [8]. The ATP-dependent Ca^{2+}-transport activities of four different membrane samples (populations *l'*, *h* and *e* and fraction III,6) shared several characteristics, i.e., they had similar K_m values, they were stimulated to a similar extent by oxalate, and they were inhibited to a similar extent by the calmodulin antagonist, calmidazolium. However, the Ca-ATPase mediating Ca^{2+} transport in the basolateral membranes (population *l'*) may differ fundamentally from that in the endoplasmic reticulum membranes, since it had a markedly lower affinity for vanadate. The conclusion that the plasma membrane Ca^{2+} pump ATPase differs from that of the endoplasmic reticulum is, in principle, consistent with results obtained with other cells types, although the nature of the differences seems to vary from one tissue to another [13,14,19,20]. The observation that Golgi-associated Ca^{2+}-transport activity had an intermediate affinity for vanadate (Table IV) suggests the possibility that the activity in this sample reflected contributions by both types of enzyme, and it leads us to speculate that the Golgi complex is an important site in the recycling of the plasma membrane Ca^{2+}-pump ATPase. Such a suggestion is certainly consistent with the results of morphological studies of membrane recycling [21,22]. We should point out, however, that within the limitations of our methodology, the Golgi-associated ATP-dependent Ca^{2+}-transport activity appeared to be concentrated in the less mature, or cis-most elements. This conclusion is drawn from the data presented in Fig. 4. Population *b* in Fig. 4 was the locus at which galactosyltransferase was most highly enriched (i.e. 18.7-fold) and therefore the population most likely to have been derived from the trans-most elements of the Golgi complex.

The inherent limitations of the fractionation approach prevent us from proposing a quantitative map of the subcellular distribution of ATP-dependent Ca^{2+}-transport activity. That is, one cannot know how faithfully the kinetic properties of an enzyme measured in an isolated membrane sample reflect the properties of that enzyme in situ. This is an especially troublesome question for a transport enzyme, since our ability to measure catalytic activity depends on vesicle orientation and sealing as well as on the integrity of the enzyme itself. The V_{max} value of 3.8 nmol Ca^{2+}/mg protein per min in population *l'* was roughly 2.5-fold lower than the values obtained in basolateral membrane samples isolated by other procedures [1,10]. This difference suggests that the isolation scheme we have employed in our attempt to resolve various membrane populations may have resulted in a greater than usual degradation of the basolateral membrane-associated Ca^{2+}-transport activity. In contrast, the V_{max} values measured in populations *e* and *h* exceed the values reported for Golgi [12] and crude endoplasmic reticulum [11] samples by factors of 3.1 and 3.4. Although we have achieved relatively better preservation of the intracellular transport activities than was possible in previous studies, we still cannot know what our yields have actually been. With these reservations in mind, it is of interest to point out that the isolated basolateral membrane populations *l'* and *l''* together account for at most 25%

of the recovered ATP-dependent Ca^{2+}-transport activity. Density window III, which contained the basolateral membrane populations during the first density gradient centrifugation step, accounted for at most 50% of the recovered activity. When this window was subfractionated, either by countercurrent distribution or by a second density gradient centrifugation procedure, the basolateral membrane populations again accounted for at most 50% of the activity recovered from the separation procedure. These are, in fact, generous estimates of the fraction of the recovered activity that can be attributed to the basolateral membranes, since populations *l'* and *l''* were overlapped by population *m* and by population *n* in the second density gradient centrifugation depicted in Fig. 6. Thus, in addition to demonstrating that ATP-dependent Ca^{2+}-transport activity has a complex distribution within intestinal epithelial cells, our study raises the possibility that the basolateral membranes might account for a relatively minor portion of the cell's Ca^{2+}-pumping ability.

Acknowledgements

The authors would like to thank Dr. Gary M. Gray for determinations of galactosyltransferase activity. This work was supported by the Netherlands Organization for Basic Research (ZWO) via FUNGO (13-37-39) and by NIH Grant EY 05801.

References

1 Ghijsen, W.E.J.M., de Jong, M.D. and van Os, C.H. (1982) Biochim. Biophys. Acta 689, 327–336
2 Hildmann, B., Schmidt, A. and Murer, H. (1982) J. Membrane Biol. 65, 55–62
3 Nellans, H.H. and Popovitch, T.E. (1981) J. Biol. Chem. 256, 9932–9936
4 Donowitz, M., Cusolito, S., Battisti, L. and Sharp, G.W.G. (1983) Am. J. Physiol. 245, G780–G785
5 Mircheff, A.K., Ahnen, D.J., Islam, A., Santiago, N.A. and Gray, G.M. (1984) J. Membrane Biol. 83, 95–107
6 Albertson, P.A. (1970) Sci. Tools 17, 53–57
7 Albertson, P.A., Andersson, B., Larsson, C. and Akerrlund, H.E. (1982) Methods Biochem. Anal. 28, 115–150
8 Ahnen, D.J., Mircheff, A.K., Santiago, N.A., Yoshioka, C. and Gray, G.M. (1983) J. Biol. Chem. 258, 5960–5966
9 Mircheff, A.K., Conteas, C.N., Lu, C.C., Santiago, N.A., Gray, G.M. and Lipson, L.G. (1983) Am. J. Physiol. 245, G133–G142
10 Van Corven, E.J.J.M., Roche, C. and van Os, C.H. (1985) Biochim. Biophys. Acta 820, 274–282
11 Rubinoff, M.J. and Nellans, H.N. (1985) J. Biol. Chem. 260, 7824–7828
12 Walters, J.R.F., Horvath, P.J. and Weiser, M.M. (1984) in Calcium and Phosphate Transport: Molecular and Cellular Aspects (Bronner, F. and Peterlik, M., eds.), pp. 187–192, Alan R. Liss, New York
13 Wibo, M., Morel, N. and Godfraind, T. (1981) Biochim. Biophys. Acta 649, 651–660
14 Colca, J.R., Kotagal, N., Lacy, P.E. and McDaniel, M.L. (1983) Biochim. Biophys. Acta 729, 176–184
15 Raeymakers, L., Wuytack, F. and Casteels, R. (1985) Biochim. Biophys. Acta 815, 441–454
16 Mircheff, A.K. and Lu, C.C. (1984) Am. J. Physiol. 247, G651–G661
17 Mircheff, A.K., Hives, H.E., Yee, V.J. and Warnock, D.G. (1984) Am. J. Physiol. 246, F853–F858
18 Mircheff, A.K., Lu, C.C. and Conteas, C.N. (1983) Am. J. Physiol. 245, G661–G667
19 Wülfroth, P. and Petzelt, C. (1985) Cell Calcium 6, 295–310
20 Famulski, K.S. and Carafoli, E. (1984) Eur. J. Biochem. 141, 15–20
21 Farquhar, M.G. and Palade, G.E. (1981) J. Cell Biol. 91, 773–1035
22 Pastan, I.H. and Willingham, M.C. (1981) Science 214, 504–509